Published in final edited form as:
Chem Biol Drug Des. 2009 October ; 74(4): 358–368. doi:10.1111/j.1747-0285.2009.00866.x.

High-content analysis of cancer-cell specific apoptosis and inhibition of *in vivo* angiogenesis by synthetic (−)-pironetin and analogs

Andreas Vogt[1,5,*], **Peter A. McPherson**[1], **Xiaoqiang Shen**[2], **Raghavan Balachandran**[3], **Guangyu Zhu**[2], **Brianne S. Raccor**[2], **Scott G. Nelson**[2], **Michael Tsang**[4], and **Billy W. Day**[2,3,5]

[1] Department of Pharmacology and Chemical Biology, University of Pittsburgh, Pittsburgh, Pennsylvania 15260

[2] Department of Chemistry, University of Pittsburgh, Pittsburgh, Pennsylvania 15260

[3] Department of Pharmaceutical Sciences, University of Pittsburgh, Pittsburgh, Pennsylvania 15260

[4] Department of Microbiology and Molecular Genetics, University of Pittsburgh, Pittsburgh, Pennsylvania 15260

[5] University of Pittsburgh Drug Discovery Institute, University of Pittsburgh, Pittsburgh, Pennsylvania 15260

Abstract

The natural product (−)-pironetin is a structurally simple small molecule microtubule (MT) perturbing agent whose biological activities appear to be exquisitely dependent on defined stereochemistry and the presence of an eletrophilic α,β-unsaturated lactone moiety. We used alkaloid-catalyzed acyl halide-aldehyde cyclocondensation (AAC) reactions in asymmetric total syntheses of (−)-pironetin and three synthetic analogs, and evaluated their biological activities by high-content analysis in cell culture and in a zebrafish model. Synthetic (−)-pironetin and 2,3-dihydro-3-hydroxypironetin caused mitotic arrest and programmed cell death in human lung cancer cells but not in normal lung fibroblasts, had nanomolar growth inhibitory activity in multidrug resistant cells, and inhibited neovascularization in zebrafish embryos. Synthetic (−)-pironetin delayed the onset but increased the extent of tubulin assembly *in vitro*. The data illustrate the power of AAC to generate biologically active synthetic analogs of stereochemically complex targets and suggest that (−)-pironetin and 2,3-dihydro-3-hydroxypironetin possess unique properties that may bestow them with advantages over existing MT-perturbing agents in the context of a whole organism or under conditions of multi-drug resistance.

Keywords

pironetin; high-content screening; multidrug resistance; zebrafish; angiogenesis

Introduction

Drugs that interfere with microtubule (MT) dynamics are among the most successful antineoplastic agents, making cellular MTs one of only a few validated anticancer targets (1).

Corresponding author: Andreas Vogt, Department of Pharmacology and Chemical Biology, University of Pittsburgh Drug Discovery Institute, 10047 Biomedical Science Tower 3, University of Pittsburgh, Pittsburgh, PA 15260; Telephone: 412-383-5856; Fax: 412-648-9009; avogt@pitt.edu.

Despite the successes with paclitaxel or the vinca alkaloids, the search for new and improved MT perturbing agents continues because of problems with solubility, toxicity and drug resistance. Many MT perturbing agents are substrates for the ABCB1 (MDR1; P-glycoprotein; Pgp) transporter (2). MT perturbing agents that are not substrates for the Pgp pump such as the epothilones (3) are promising candidates for development of improved antineoplastic therapies. Many MT perturbing agents are complex natural products that have evolved to fit into defined sites on their respective protein target. Total syntheses typically involve numerous steps and synthetic tractability is often a limiting factor in drug discovery and development. MT perturbing agents frequently violate empirical rules used in drug development, such as the "rule of 5" requirements of low molecular weight and hydrophobicity (4). Agents with simplified structures could therefore be advantageous for pharmacokinetic and logistical reasons.

An interesting small molecule with MT perturbing properties is the polypropionate (−)-pironetin ((5*R*,6*R*)-5-ethyl-6-((2*R*,3*S*,4*R*,5*S*,*E*)-2-hydroxy-4-methoxy-3,5-dimethylnon-7-enyl)-5,6-dihydro-2*H*-pyran-2-one) (**1**) (Figure 1). (−)-Pironetin was isolated from a bacterial broth of *Streptomyces* sp. NK10958 (5) and reported as a natural product inhibiting plant growth. (−)-Pironetin is toxic to cancer cells in culture, arrests cells in G2/M, and has shown moderate antitumor activity in the 388 leukemia model (6). Pironetin induces, like many antimitotic agents, apoptosis that is associated with phosphorylation of Bcl-2 and Bcl-x_L phosphorylation (7). (−)-Pironetin binds to isolated tubulin and prevents tubulin assembly *in vitro* (7), presumably by covalent modification of a unique binding site on the α-subunit of the tubulin heterodimer (8).

The chemical structure of (−)-pironetin is relatively simple but it appears that the biological activities of (−)-pironetin are exquisitely dependent on defined stereochemistry at six asymmetric centers. With the exception of C7, which has been shown to be critical for biological activity, little is known about the relative importance of the other centers. This is in part due to a lack of synthetic routes that permit complete control over stereochemical outcomes. While several groups have reported total syntheses of (−)-pironetin (9–12), investigations of the biological activities of (−)-pironetin were performed using the natural product isolated and purified from bacterial broth. The limited number of reports that have described the effects of chemical modifications on (−)-pironetin's biological activity (8,10) mostly utilized semisynthetic materials derived from the natural product. Removal of a methyl group to give demethylpironetin appears to be tolerated, while reversal of configuration on C7 and reduction of the double bond in the lactone ring to give the 2,3-dihydro derivative results in at least 1000-fold loss of biological activity (10). Recent studies support a model of covalent interaction between pironetin and its molecular target, presumably through nucleophilic addition of the amino side chain of α-tubulin lysine 352 to the α,β-unsaturated lactone moiety (8). While these findings demonstrate a unique target site of action for (−)-pironetin, chemical reactivity is generally seen as a liability in drug development, and non-electrophilic agents would be predicted to have more favorable pharmacological properties.

We recently reported an asymmetric synthesis of (−)-pironetin using alkaloid-catalyzed acyl halide-aldehyde cyclocondensation (AAC) (13). Here, we exploited this successful total synthesis to synthesize the optical antipode of the natural product, (+)- pironetin (**2**), and two novel analogs with modifications in the α,β-unsaturated lactone ring. Evaluation of the biological activities of these synthetic pironetins by high-content analysis demonstrated that (−)-pironetin and its 2,3-dihydro-3-hydroxy analogue **3** caused mitotic arrest and inhibited the growth of cancer cells in culture at submicromolar concentrations. Both compounds retained activity against multidrug resistant cells, caused cancer-cell specific apoptosis and had antiangiogenic activity in a zebrafish model.

Methods and Materials

Synthesis

Compounds **5–15** and (−)-pironetin **1** were prepared according to the published procedures (13). The synthesis of **3** and **4** is described below. Full details of experimental procedures and characterization for (+)-pironetin **2** and its synthesis intermediates are provided in the Supplemental Data Section.

(*E*,3*S*,4*S*,5*R*,7*R*,8*S*,9*R*,10*S*)-2,3-Dihydro-3-hydroxypironetin (3)

A solution of ester **5** (0.9 mg, 1.7 μmol) in CH_2Cl_2 (25 μL) 0 °C was treated with trifluoroacetic acid (4 μL, ~2 μL/μmol **5**). The resulting solution was allowed to stand at 0 °C with periodic agitation for 2 h, whereupon the volatiles were evaporated in vacuo and the resulting crude product mixture was purified by filtration through a small plug of silica gel (7:3 hexanes-ethyl acetate) to afford the title compound (0.7 mg) as a colorless foam. ^{1}H NMR (300 MHz, $CDCl_3$) δ 5.51–5.32 (m, 2H), 4.74 (m, 1H), 4.37–4.32 (m, 1H), 4.21 (br d, 1H), 3.51 (s, 3H), 3.50 (d, *J* = 2.3 Hz, 1H), 3.10 (dd, *J* = 6.1, 4.4 Hz, 1H), 2.92 (dd, *J* = 18.4, 5.4 Hz, 1H), 2.71 (dd, *J* = 18.3, 3.0 Hz, 1H), 2.34–2.25 (m, 1H), 2.15 (br, 1H), 2.10–2.01 (m, 1H), 2.00–1.90 (m, 2H), 1.87–1.80 (m, 1H), 1.74–1.64 (m, 3H), 1.67 (d, *J* = 5.3 Hz, 3H), 1.61–1.47 (m, 1H), 1.01 (d, *J* = 7.1 Hz, 3H), 0.98 (t, *J* = 7.4 Hz, 3H), 0.94 (d, *J* = 6.9 Hz, 3H); HRMS (ESI) *m/z* calcd for $C_{19}H_{34}O_5Na$: 365.2304; found: 365.2295. Reanalysis by LC-MS (ESI) after repeated use and > 12 months of storage in DMSO at −20C confirmed the identity of **3** as a major TIC peak with a retention time of 11.12 min. (+Q1, *m/z 343.2 (M+H); 365,3 (M+Na))* and showed no significant contamination with (−)-pironetin (retention time 11.98 min; +Q1, *m/z 325.3 (M +H); 347,3 (M+Na))* (see Supporting Information for details).

(*E*,4*S*,5*R*,7*R*,8*S*,9*R*,10*S*)-3-Hydroxypironetin (4)

A solution of ester **6** (1.1 mg, 2.1 μmol) in CH_2Cl_2 (25 μL) at 0 °C was treated with trifluoroacetic acid (5 μL, ~2 μL/μmol **6**). The resulting solution was allowed to stand at 0 °C with periodic agitation for 2 h, whereupon the volatiles were evaporated in vacuo and the resulting crude product mixture was purified by filtration through a small plug of silica gel (7:3 hexanes-ethyl acetate) to afford the title compound (0.7 mg, 100%) as a colorless foam. ^{1}H NMR (300 MHz, $CDCl_3$) δ 5.51–5.32 (m, 2H), 5.19 (s, 1H), 4.70 (m, 1H), 4.29 (brd, 1H), 3.48 (s, 3H), 3.43 (d, *J* = 2.3 Hz, 1H), 3.09 (dd, *J* = 6.1, 4.4 Hz, 1H), 2.58 (ddd, *J* = 7.4, 7.2, 3.4, 1 H), 2.13–2.04 (m, 1H), 1.90–1.81 (m, 2H), 1.82–1.74 (m, 1H), 1.70–1.63 (m, 3H), 1.67 (d, *J* = 5.3 Hz, 3H), 1.58–1.46 (m, 1H), 1.00 (d, *J* = 7.1 Hz, 3H), 0.97 (t, *J* = 7.4 Hz, 3H), 0.96 (d, *J* = 6.9 Hz, 3H); HRMS (ESI) *m/z* calcd for $C_{19}H_{32}O_5Na$: 363.2147; found: 363.2140.

HCS reagents

Anti-phospho-histone H3 (Ser10) was from Upstate. Cleaved caspase antibody (5A1, Asp175, rabbit monoclonal) was from Cell Signaling. Sheep anti-p53 antibody was from EMD Biosciences (formerly Calbiochem). FITC-labeled donkey anti-mouse IgG, Cy3-labeled donkey anti-rabbit IgG and Cy5-labeled donkey anti-sheep IgG were from Jackson Immunoresearch. AlexaFluor 488-conjugated goat-anti-mouse and AlexaFluor555-conjugated goat-anti-rabbit IgG were from Molecular Probes (Invitrogen). All other reagents including standard agents and mouse monoclonal anti-α-tubulin antibody were from Sigma, St. Louis, MO.

Cells and culture

HeLa, A549 and IMR-90 human cancer cells (ATCC), and DC3F and VCRd5L Chinese hamster cells (a gift from June L. Biedler when at Memorial Sloan-Kettering Cancer Center) were maintained in Dulbecco's minimum essential medium (DMEM) containing 10% fetal

bovine serum (FBS, HyClone, Logan, UT) and 1% penicillin-streptomycin (Life Technologies, Inc., Rockville, MD) in a humidified atmosphere of 5% CO_2 at 37°C. The human breast cancer cell lines MDA-MB231 (ATCC) and MCF-7 (28^{th} passage cells, a generous gift from Dr. Marc Lippman when at the Lombardi Cancer Center) and the T98G glioma cancer cells (a gift from Dr. Ian Pollack, University of Pittsburgh) were maintained in RPMI1640 with 10% FBS, 1% penicillin and 1% glutamine.

Automated high content cellular analyses

The effects of pironetin analogs on mitotic arrest and cellular microtubules were performed exactly as described (14,15). Briefly, HeLa human cervical carcinoma cells treated with vehicle (DMSO) or ten two-fold concentration gradients of test agents for 20 h were labeled with Hoechst 33342 and incubated with a primary antibody cocktail followed by fluorescently labeled secondary antibodies. The conditions for the mitotic index assay have been described in detail (14). For the apoptosis/p53 assay, cells were incubated with rabbit monoclonal anti-cleaved caspase-3 (1:500) and sheep polyclonal anti-p53 (1:500), followed by a mixture of Cy3-labeled donkey anti-rabbit IgG (1:250) and Cy5-labeled donkey anti-sheep IgG (1:250). Microplates were analyzed with an ArrayScanII (Cellomics, Pittsburgh, PA) using the Compartmental Analysis Bioapplication exactly as described (14). With the exception of DNA content, which represents the integrated (total) Hoechst 33342 fluorescence intensity of all the pixels in the nucleus, all measurements are the average pixel intensity in an area defined by the nuclear mask. For determination of mitotic index, nuclear condensation and p53 nuclear accumulation, thresholds for Hoechst, phospho-histone-H3 and p53 intensities were defined as the average intensity plus one standard deviation from vehicle-treated wells. Cells were classified as positive if their average Hoechst, Cy3, or Cy5 intensity exceeded this threshold. To visually illustrate the effects of test agents on cellular microtubules and mitotic arrest, HeLa cells were plated in 8-well chamber slides (Falcon Biocoat) and immunostained as described for the mitotic index assay, except that secondary antibodies were replaced by AlexaFluor 488-conjugated goat-anti-mouse and AlexaFluor 555-conjugated goat-anti-rabbit secondary antibodies.

Antiproliferative activities

Two independent methods were used to assess growth inhibitory activity. For MCF-7 breast cancer and T98G glioma cells, a three day MTS assay was performed (14). Cells were seeded into 96-well plates in RPMI 1640 with 10% FBS, allowed to attach and grow for 48 h, then treated for 72 h with fresh RPMI1640 (without phenol red) containing 10% FBS. 1% penicillin, 1% glutamine and either DMSO (1%; N = 8) or a range of concentrations of test agents dissolved in DMSO (1%; N = 4 per concentration). Cell number was determined spectrophotometrically at 490 nm minus absorbance at 630 nm after exposure to 3-(4,5-dimethylthiazol-2-yl)-5-(3-carboxymethoxyphenyl)-2-(4-sulfophenyl)-2*H*-tetrazolium and *N*-methylphenazine methylsulfate. The fifty percent growth inhibitory concentrations (GI_{50}) of test agents were calculated from the spectrophotometrically determined growth of the control cells over the 72 h period.

For MDA-MB231 breast cancer, A549 lung cancer, and DC3F and VCRd5L Chinese hamster cells, we used our previously described image-based analysis procedure (16). Briefly, cells were plated at low density (500 – 2000 cells/well) in 384-well microplates, allowed to attach overnight and treated with test agents. After four days of continuous exposure to compounds, cells were labeled with Hoechst 33342 and nuclei enumerated on the ArrayScanII. Acquisition parameters were set such that the instrument acquired a minimum of 5,000 cells in each well. Cell densities were calculated as objects per imaging field and normalized to vehicle control density at the end of the study. DC3F and VCRd5L Chinese hamster cells grew faster than the human cancer cells, limiting the duration of compound exposure to three days.

Inhibition of tubulin assembly

Electrophoretically homogeneous bovine brain tubulin (final concentration 10 μM; 1 mg/mL) was preincubated with test agents dissolved in DMSO (4% final concentration) and monosodium glutamate (0.8 M final concentration) for 15 min at 30 °C. The reaction mixture was cooled to 0 °C and GTP (0.4 mM final concentration) was added. Reaction mixtures were transferred to cuvettes held at 2.5 °C in a spectrophotometer reading absorbance (turbidity) at 350 nm. Baselines were established and temperature was quickly raised to 30 °C (in approximately 1 min). After 20 min, the temperature was returned to 2.5 °C.

Radioligand displacement studies

Each 0.32 mL reaction mixture contained 5 μM inhibitor, 10 μM [^{3}H]vinblastine, 10 μM bovine brain tubulin, 0.5 mM $MgCl_2$ and 1% DMSO in 0.1 M Mes, pH 6.9. The mixture was incubated for 30 min at room temperature and 0.15 mL of the reaction mixture was applied in duplicate to 2 mL Sephadex G-50 (superfine) columns. Columns were centrifuged at 800 × *g* for 4 min and the protein concentration in the effluent was determined using the bicinchoninic acid assay (17). The amount of radiolabeled ligand bound to tubulin was determined using scintillation spectrometry. Each value represents the mean ± SD of four determinations. The average stoichiometry of binding in the control reaction mixture was 0.63 mol of [^{3}H]vinblastine per mol of tubulin. Inhibition was calculated as the percent difference relative to that of the control incubation with DMSO (i.e., without test agent) assigned as 0% inhibition.

Anti-angiogenesis assay

The (*Tg(Fli1:EGFP)^{y1}*) line was obtained from Dr. Brant Weinstein and maintained as described (18). For each experiment, embryos were collected 24 hpf and staged according to (19). Five transgenic zebrafish embryos (*Tg(Fli1:EGFP)^{y1}*) were then treated in 96-well plates in 200 μl E3 medium (5mM NaCl, 0.33mM $CaCl_2$, 0.17mM KCl, 0.33mM $MgSO_4$) containing vehicle (DMSO, 0.5%), (−)- pironetin (5 μM to 0.5 μM), **3** (50μM) or SU11652 (Calbiochem) (40 μM) for 8 h or 24 h. The chorions were manually removed from treated embryos and single embryos were transferred to a 384-well plate containing 40μg/mL MS222 (tricaine methanesulfonate, Sigma) in E3 for imaging. Photomicrographs of fluorescent ISV were acquired with the ArrayScan II (Cellomics, Pittsburgh, PA) using a 2.5X objective and a GFP compatible bandpass filter set. The experiments were repeated at least two times to show reproducibility.

Results and Discussion

Synthesis of pironetins

Our successful asymmetric total synthesis of (−)-pironetin provided the source of natural product required for biological testing (13). (+)-Pironetin was prepared using a synthesis sequence identical to that affording (−)-pironetin save for, where applicable, the use of enantiomeric or pseudoenantiomeric reaction catalysts (see Supporting Information).

The 3-hydroxy and 2,3-dihydro-3-hydroxy pironetins constituted two novel structures easily available from our existing synthesis suitable for evaluating hypotheses concerning pironetin's mode of action. Covalent tubulin modification via conjugate addition of a suitably position lysine residue (Lys352) at the tubulin binding site has been proposed as triggering event in (−)-pironetin's anti-tubulin activity (8) (Figure 1B). Based on this hypothesis, we were interested in determining if derivatives with natural stereochemistry and a substituent allowing H-bonding interaction at C3 for the putative conjugate addition would retain activity. We were attracted to pironetin derivatives that could engage the lysine residue in an H-bond donor-acceptor interaction but that would be immune to the conjugate addition event believed responsible for

the natural product's activity. We targeted **3** and **4** as derivatives of interest, each possessing a C3 hydroxyl function as a hydrogen bond donors and having limited or no capacity as Michael acceptors.

β-Ketoester **5**, prepared in the course of the (−)-pironetin total synthesis, functioned as the common intermediate for preparing both **3** and **4** (Figure 1B). To access **3**, the β-keto ester **5** was first reduced ($NaBH_4$) to the diastereomeric mixture of β-hydroxy esters **6**. The mixture was reacted with TsOH (THF, 23 °C) to affect lactonization and silyl ether cleavage to generate the mixture of C3 epimers of 2,3-dihydro-3-hydroxypironetin **3**. Reacting **5** with TFA to affect removal of the *t*-butyl ester proceeded with concomitant lactonization and tautomerization to afford **4**.

High-content analysis of mitotic arrest by pironetin analogs

We used our previously described multiparameter high-content analysis (20) to investigate the effects of the four synthetic pironetins **1**–**4** (Figure 1) on cellular microtubule perturbation and mitotic arrest. Asynchronously growing HeLa cells were treated with compounds in collagen-coated 384 well microplates and immunostained with antibodies against α-tubulin and phospho-histone H3. Nuclei were counterstained with Hoechst 33342. Figures 2A–C show the quantitative assessment of MT perturbation and mitotic arrest. (−)-Pironetin potently induced mitotic arrest as measured by chromatin condensation (Figure 2B) and an increase in the percentage of cells with elevated phospho-histone H3 (Figure 2C), with activity comparable to those of the standard agents vincristine and paclitaxel. The optical antipode **2** and the 3-hydroxy derivative **4** were at least three orders of magnitude less active (Figure 2 and Supplemental Table 1). Interestingly, 2,3-dihydro-3-hydroxypironetin **3** retained submicromolar activity despite lacking the unsaturated lactone moiety. The data suggest that either the reactive double bond in the lactone portion of (−)-pironetin is not required for biological activity, making **3** the first non-electrophilic pironetin with submicromolar activity, or that **3** is a prodrug that is converted by cells to (−)-pironetin by cellular dehydrating enzymes.

Loss of tubulin immunostaining in cells treated with MT destabilizing agents

The two active pironetins and vincristine initially increased well average tubulin immunostaining intensity (Figure 2A). At higher concentrations, tubulin staining intensity decreased, indicating a loss of cellular MT mass. This biphasic response appears to be typical for MT destabilizing agents (20) but the reasons for this phenomenon are not fully understood. To investigate potential sources for the apparent loss of MT mass, we analyzed tubulin content and histone H3 phosphorylation at concentrations of compounds that decreased MT mass compared with paclitaxel (200 nM vincristine, 100 nM pironetin and 2.5 μM **3**). Vincristine, (−)-pironetin and **3** caused a heterogeneous cell response with two major cell populations (Figure 2D–G). A substantial proportion of the cells showed signs of mitotic arrest, namely bright, condensed nuclei, high levels of phospho-histone H3, and morphological changes (cell rounding) that obscured visual evaluation of MT morphology. The other cell subpopulation remained flatly attached to the microplate, had low levels of phospho-histone H3, disorganized MTs and possibly less intense tubulin immunostaining than vehicle treated control cells. In contrast to previously presented images (8), (−)-pironetin-treated cells also contained what appeared to be tubulin aggregates that were visible in the flat, attached cells but obscured by rounding in the mitotic cells (Figure 2F). We therefore wished to investigate whether the loss of tubulin mass at higher concentrations of vincristine and (−)-pironetin originated occurred in mitotic cells, interphase cells, or both. A detailed single-cell analysis revealed that the loss of microtubule mass at high compound concentrations was a result of decreased tubulin immunostaining in both mitotic cells (compare yellow symbols (VCR) vs red symbols (PTX) in the upper right hand quadrant in Fig 2H) and in interphase cells (compare yellow symbols (VCR) to red symbols (PTX) and grey symbols (vehicle) in the lower left hand quadrant in

Figure 2H). In contrast, the MT stabilizer paclitaxel, which did not show reversal of MT mass increases, had much higher levels of MT staining (Figure 2H and 2I, red circles). Thus, single-cell analysis demonstrated loss of MT mass in mitotic cells, thereby eliminating measurement ambiguities caused by changes in cell morphology, and distinguished MT-perturbing agents by mode of action. The data favor a mechanism of action for vincristine, (−)-pironetin and **3** that involves MT depolymerization rather than stabilization and support the hypothesis put forth by Giuliano (15) that in cells treated with MT destabilizing agents some of the tubulin becomes monomeric and is partially extracted into assay buffers during permeabilization and immunostaining.

Antiproliferative activity in human cancer and multidrug-resistant Chinese hamster cells

(−)-Pironetin has been reported to inhibit the growth of cancer cells in culture at nanomolar concentrations. It has also been reported to be active against human small cell lung cancer H69 cells, including two cell lines resistant to the β-tubulin-targeted drugs vindesine (H69/VDS) and paclitaxel (H69/Txl). Pironetin was also reported to inhibit the growth of human leukemic K562 multidrug-resistant cells (K562/ADM), which have *MDR1* gene expression, as potently as the parental K562 cells (21). We therefore tested our synthetic pironetin analogs for inhibition of cell growth using four different human cancer cell lines and the DC-3F and VCRd5L multidrug resistant chinese hamster cell line pair that has been extensively used and is well described in the literature (22). As expected, synthetic (−)-pironetin potently inhibited the growth of human breast cancer, lung cancer, and glioblastoma cells (Table 1). Consistent with the HCS data presented in Figure 2 and Table S1, **3** retained submicromolar activity whereas **2** and **4** were at least three orders of magnitude less active. Importantly, the VCRd5L cells, which were resistant to vincristine and paclitaxel, remained sensitive to (−)-pironetin and **3**.

Inhibition of tubulin assembly *in vitro*

It has been reported that (−)-pironetin isolated from bacterial broth inhibits MT assembly *in vitro* and may even be able to dissolve pre-formed MTs (7). We therefore investigated the effects of synthetic pironetin *in vitro* and found it delayed the onset but increased the extent of tubulin assembly (Figure 3B). Polymer formation by (−)-pironetin was concentration-dependent and occurred in the absence of GTP (Figure 3C). Polymer formed by (−)-pironetin was cold stable (Figure 3C). Surprisingly, synthetic pironetin did not dissolve pre-formed MTs under the experimental conditions used (Figure 3D). Thus, the effects of (−)-pironetin on isolated tubulin were quite different from that of vinblastine (Figure 3A) and from those reported previously for the natural product (7). The data are, however, consistent with the formation of tubulin aggregates in intact cells (Figure 2), which were not visible in images presented for natural (−)-pironetin (7) or a semisynthetic biotinylated derivative (8). Thus, it appears that synthetic (−)-pironetin has unique effects on tubulin *in vitro* and on cellular MTs that were not previously seen with material from natural sources. Interestingly, **3** (40 μM) lacked the ability to inhibit tubulin assembly *in vitro* and did not induce formation of tubulin polymer (data not shown).

Competition for binding the vinca domain

Further evidence that (−)-pironetin is mechanistically distinct from the vinca alkaloids was provided by an inhibition assay utilizing [^{3}H]vinblastine as the radiolabeled tracer. Vincristine and dolastatin 10 are well known inhibitors of [^{3}H]vinblastine binding (23) and served as positive controls in the assay. As shown in Table 2, 5 μM vincristine or dolastatin 10 inhibited the binding of 10 μM [^{3}H]vinblastine to tubulin by 65 + 2 and 61 + 1%, respectively. Of the pironetins, only (−)-pironetin weakly inhibited the binding of [^{3}H]vinblastine (Table 2). Neither the analogues of pironetin nor the optical antipode had any appreciable binding

inhibitory activity at 5 μM. These results coincide with those previously reported by Kondoh et al., although their results suggest a higher percentage of inhibition by (−)-pironetin (7). This may be due to the differences in the amounts of protein, tracer and inhibitor that were used in the two experiments. In our inhibition assay, the tubulin-tracer-inhibitor molar ratio used was 2:2:1, i.e., a substoichiometric amount of inhibitor. We performed our experiments with this ratio because it provided a rapid and validated method of comparing the positive controls, including historical values obtained for them, to the test compounds. This is in contrast to Kondoh's assay, which was performed with a large excess of inhibitor, at a tubulin-tracer-inhibitor molar ratio of 100:1:1000, inflating the apparent inhibition. It has been suggested that (−)-pironetin forms a covalent bond to Lys352 on α-tubulin, which is found near the interface of the longitudinal contacts made by tubulin heterodimers (8). This places (−)-pironetin in proximity to the nucleotide exchangeable site on the adjacent longitudinal β-tubulin, the site at which vinca alkaloids bind (24). The results from both our and Kondoh's [^{3}H]vinblastine competitive binding assays are in agreement with this proposed binding site for (−)-pironetin, as covalent linkage of (−)-pironetin to αLys352 on a free tubulin heterodimer constructs a modified protein that would compete with [^{3}H]vinblastine for its binding site, the solvent- (and incoming heterodimer-) accessible portion of β-tubulin on the plus end of a protofilament.

Induction of cancer-cell specific cell cycle arrest and apoptosis

We next investigated effects of compounds on cell cycle distribution and apoptosis in normal and in cancer cells. We chose IMR-90 human lung fibroblasts because they are a well characterized normal cell line that is resistant to a variety of cytotoxic and antisignaling agents (25,26). The cells have a finite lifespan of approximately 60 population doublings (27) before entering crisis, which we confirmed (data not shown). Cells were plated in 384 well microplates as described for the mitotic index assay and treated for 20h with pironetin, **3**, or the standard agents paclitaxel and vincristine. Cells were fixed, stained with Hoechst 33342 and a cleaved caspase-3 antibody, and analyzed for DNA content, apoptotic morphology and caspase cleavage by HCS. HeLa cells treated with pironetin or **3** arrested in G2/M whereas normal IMR-90 lung fibroblasts retained the G0/G1 bias seen in the absence of drug treatment (Figure 4A). A-549 lung cancer cells also accumulated in G2/M (data not shown). Enumeration of cells that remained attached to the microplate after compound treatment demonstrated a cell loss in the two human cancer cell lines but not in the normal cells (Figure 4B, *Cell density*). Both cancer cell lines underwent apoptosis as measured by changes in nuclear morphology (Figure 4B, *Chromatin condensation*). To ascertain that the nuclear morphology response was not solely a result of mitotic arrest, we included caspase-3 activation as a second, independent marker of apoptotic cell death (Figure 4B, *Caspase cleavage*). In the A-549 cells, both (−)-pironetin and **3** induced nuclear accumulation of p53 (Figure 4B, *p53 induction*). In contrast, no changes in nuclear morphology, caspase activation, or p53 induction were detected in IMR-90 cells. Similar results were observed with paclitaxel and vincristine. To confirm that IMR-90 cells had an intact p53 response, cells were treated with camptothecin, which induced p53 with similar potency in normal and cancer cells (Figure S3). As expected for a DNA damaging agent in p53 wild-type cells, camptothecin did not cause nuclear condensation or caspase cleavage in A-549 cells (Figure S1), indicating that these cells underwent cell cycle arrest rather than programmed cell death. To ascertain that IMR-90 cells had an intact apoptotic response, we treated cells with phenylarsine oxide (PAO), a non-specific, thiol-poisoning noxious agent (28), which caused apoptosis to a similar or greater extent in IMR-90 compared with A-549 cells (Figure S3). The data indicate that pironetin and **3** are capable of selectively killing transformed cells irrespective of p53 status, a desirable property that (−)-pironetin and **3** shared with the clinically used vincristine and paclitaxel.

Inhibition of angiogenesis in zebrafish embryos

Solid tumors require an adequate supply of blood vessels to survive, grow, and metastasize (reviewed in (29)). The ability to inhibit neovascularization is a desired attribute for novel antineoplastic agents, and drugs with anti-angiogenic activity are currently in clinical cancertrials (30). Because the vascular system has been well described and shown to be highly conserved between vertebrates (31), the zebrafish has become a well accepted model for studies of vertebrate developmental biology including blood vessel formation (32,33). We have recently developed an image analysis method to quantify ISV development in fluorescent zebrafish embryos using a Cognition Network Technology ruleset(34), and applied it to embryos treated with MT perturbing agents including 2-methoxyestradiol and (−)-pironetin. While both MT perturbing agents stunted ISV development, their concentration response curves were steep and at higher concentrations embryos appeared smaller in size, suggesting non-specific growth suppression (data not shown). We therefore investigated whether **3** retained (−)-pironetin's ability to inhibit angiogenesis and if so, whether the lack of the α,β-unsaturated lactone would reduce the non-specific effects.

We used *Tg(fli1:EGFP)*^{y1}, a transgenic line that expresses EGFP under the control of the *Fli1* promoter (35). Because the *Fli1* gene is expressed in endothelial cells, EGFP expression labels all blood vessels, thus providing a live visual marker for vascular development. *Tg (fli1:EGFP)*^{y1} zebrafish embryos were treated at 24 hpf with (−)-pironetin or **3** and kept in medium for 8 h or 24 h. Vehicle-treated embryos developed a vascular system including well-established intersegmental vessels (ISV) that extend from the dorsal aorta (DA) and connect to the dorsal longitudinal anastomotic vessel (DLAV) (Figure 5A, (31)). In contrast, ISV outgrowth from the dorsal aorta was severely stunted in (−)- pironetin treated embryos and prevented the establishment of the DLAV at the dorsal region of the embryo. Consistent with the results from the automated analysis(34), 2.5 μM (−)-pironetin fully inhibited ISV growth (Figure 5B) without obvious signs of toxicity such as the appearance of necrotic opaque cells. We observed a bent tail phenotype at higher concentrations (5μM, data not shown) that suggests that at this concentration (−)-pironetin would likely cause embryo lethality. Compound **3** retained the ability to inhibit ISV growth but was about 20-fold less active than (−)-pironetin (Figure 5C). Embryos treated with an equipotent dose of **3** showed little difference in gross morphology compared with (−)-pironetin. (Figure 5B and 5C). Morphometric measurements of embryo length and area obtained with the Cognition Network Technology ruleset (34) showed that at 48 hpf embryos treated with (−)-pironetin and **3** were slightly smaller than vehicle treated embryos (Table S2). The VEGFR tyrosine kinase inhibitor, SU11652, which we have recently shown to inhibit ISV growth in *Tg(fli1:EGFP)*^{y1} embryos (36) was about as potent as **3** (Figure 5D). The data indicate synthetic (−)-pironetin and **3** had antiangiogenic activity in a zebrafish model of angiogenesis at nontoxic concentrations.

Antiangiogenic activity may enhance the efficacy of cytotoxic drugs. There are numerous examples where combinations of antiangiogenic agents with chemotherapy had improved clinical outcomes (30). It has been proposed that antiangiogenic effects of paclitaxel (37) and vinblastine (38) could contribute to their *in vivo* antitumor efficacy. Thus, the combination of antiproliferative and antiangiogenic properties appears to be a desirable feature that (−)-pironetin and **3** shared with two clinically used MT-perturbing agents.

Conclusions and Future Directions

The natural product (−)-pironetin is a structurally simple antimitotic agent whose shortcomings are exquisite dependence on absolute configuration at six asymmetric centers and a reactive α,β-unsaturated lactone moiety, both of which present obstacles in the further development of (−)-pironetin as an anticancer agent. We solved the former by employing an elegant synthetic methodology termed alkaloid-catalyzed acyl halide-aldehyde cyclocondensation (AAC),

which permits complete control over all stereocenters in the assembly of repeating propionate units (13). We addressed the latter challenge by using AAC to synthesize two analogs of (−)-pironetin with modifications in the lactone portion and found that one of them, 2,3-dihydro-3-hydroxypironetin (**3**), retained much of the parent compound's potency in cellular assays making **3** the first non-electrophilic pironetin with submicromolar activity. Both agents had antiangiogenic activity in a zebrafish model of angiogenesis and did not appear to be substrates for the p-glycoprotein pump. The data suggest that the reactive double bond in the lactone portion of (−)-pironetin may not be an absolute requirement for biological activity. Collectively, the results demonstrate that pironetin and **3** are promising pharmacophores with desirable attributes with regards to antineoplastic activity from which to develop more active derivatives with enhanced pharmacokinetic and pharmacodynamic properties. The data encourage further development of pironetin analogs as potential therapeutic agents in cancer treatment.

Supplementary Material

Refer to Web version on PubMed Central for supplementary material.

Acknowledgments

We thank Dr. Brant Weinstein for the *Tg(fli1:EGFP)*^{y1} transgenic line, Dr. John S. Lazo for providing laboratory space and equipment, and Daniel Camarco, Gabriela Molina, and Vasiliy Korotchenko for excellent technical assistance. This work was supported by the National Institutes of Health [Grants CA78039 and GM63151]; the American Cancer Society [Grant RSG-00-025-04-CDD]; and the Fiske Drug Discovery Fund.

Abbreviations

Cy3	indocarbocyanine dye with three-methine linker
Cy5	indocarbocyanine with five-methine linker
DMSO	dimethylsulfoxide
DA	dorsal aorta
DLAV	dorsal longitudinal anastomotic vessel
HBSS	Hank's Balanced Salt Solution
HCS	high-content screening
hpf	hours post fertilization
ISV	intersegmental vessels
MDEC	minimal detectable effective concentration
Mes	morpholineethanesulfonate
MT	microtubules
(−)-pironetin	(5*R*,6*R*)-5-ethyl-6-((2*R*,3*S*,4*R*,5*S*,*E*)-2-hydroxy-4-methoxy-3,5-dimethylnon-7-enyl)-5,6-dihydro-2*H*-pyran-2-one
PCV	posterior cardinal vein
TMS*Qn*	*O*-trimethylsilylquinine

References

1. Jordan MA, Wilson L. Microtubules as a target for anticancer drugs. Nat Rev Cancer 2004;4:253–265. [PubMed: 15057285]

2. Szakacs G, Paterson JK, Ludwig JA, Booth-Genthe C, Gottesman MM. Targeting multidrug resistance in cancer. Nat Rev Drug Discov 2006;5:219–234. [PubMed: 16518375]
3. Chou TC, Zhang XG, Harris CR, Kuduk SD, Balog A, Savin KA, Bertino JR, Danishefsky SJ. Desoxyepothilone B is curative against human tumor xenografts that are refractory to paclitaxel. Proc Natl Acad Sci U S A 1998;95:15798–15802. [PubMed: 9861050]
4. Lipinski CA. Drug-like properties and the causes of poor solubility and poor permeability. J Pharmacol Toxicol Methods 2000;44:235–249. [PubMed: 11274893]
5. Kobayashi S, Tsuchiya K, Harada T, Nishide M, Kurokawa T, Nakagawa T, Shimada N, Kobayashi K. Pironetin, a novel plant growth regulator produced by Streptomyces sp. NK10958. I. Taxonomy, production, isolation and preliminary characterization. J Antibiot (Tokyo) 1994;47:697–702. [PubMed: 8040075]
6. Kondoh M, Usui T, Kobayashi S, Tsuchiya K, Nishikawa K, Nishikiori T, Mayumi T, Osada H. Cell cycle arrest and antitumor activity of pironetin and its derivatives. Cancer Lett 1998;126:29–32. [PubMed: 9563645]
7. Kondoh M, Usui T, Nishikiori T, Mayumi T, Osada H. Apoptosis induction via microtubule disassembly by an antitumour compound, pironetin. Biochem J 1999;340 (Pt 2):411–416. [PubMed: 10333483]
8. Usui T, Watanabe H, Nakayama H, Tada Y, Kanoh N, Kondoh M, Asao T, Takio K, Watanabe H, Nishikawa K, Kitahara T, Osada H. The anticancer natural product pironetin selectively targets Lys352 of alpha-tubulin. Chem Biol 2004;11:799–806. [PubMed: 15217613]
9. Chida N, Yoshinaga M, Tobe T, Ogawa S. Total synthesis of (−)-PA-48153C (pironetin) utilising L-quebrachitol as a chiral building block. Chem Commun 1997:1043–1044.
10. Watanabe H, Watanabe H, Usui T, Kondoh M, Osada H, Kitahara T. Synthesis of pironetin and related analogs: studies on structure-activity relationships as tubulin assembly inhibitors. J Antibiot (Tokyo) 2000;53:540–545. [PubMed: 10908119]
11. Keck GE, Knutson CE, Wiles SA. Total synthesis of the immunosupressant (−)-pironetin (PA48153C). Org Lett 2001;3:707–710. [PubMed: 11259042]
12. Dias LC, De Oliveira LG, De Sousa MA. Total synthesis of (−)- pironetin. Org Lett 2003;5:265–268. [PubMed: 12556168]
13. Shen X, Wasmuth AS, Zhao J, Zhu C, Nelson SG. Catalytic asymmetric assembly of stereodefined propionate units: an enantioselective total synthesis of (−)-pironetin. J Am Chem Soc 2006;128:7438–7439. [PubMed: 16756287]
14. Wang Z, McPherson PA, Raccor BS, Balachandran R, Zhu G, Day BW, Vogt A, Wipf P. Structure-activity and high-content imaging analyses of novel tubulysins. Chem Biol Drug Des 2007;70:75–86. [PubMed: 17683369]
15. Giuliano KA. High-content profiling of drug-drug interactions: cellular targets involved in the modulation of microtubule drug action by the antifungal ketoconazole. J Biomol Screen 2003;8:125–135. [PubMed: 12844433]
16. Vogt A, Kalb EN, Lazo JS. A scalable high-content cytotoxicity assay insensitive to changes in mitochondrial metabolic activity. Oncol Res 2004;14:305–314. [PubMed: 15206493]
17. Smith PK, Krohn RI, Hermanson GT, Mallia AK, Gartner FH, Provenzano MD, Fujimoto EK, Goeke NM, Olson BJ, Klenk DC. Measurement of protein using bicinchoninic acid. Anal Biochem 1985;150:76–85. [PubMed: 3843705]
18. Westerfield, M. A guide for the laboratory use of zebrafish (Danio rerio). Univ. of Oregon Press; Eugene: 2000. The zebrafish book.
19. Kimmel CB, Ballard WW, Kimmel SR, Ullmann B, Schilling TF. Stages of Embryonic-Development of the Zebrafish. Developmental Dynamics 1995;203:253–310. [PubMed: 8589427]
20. Wipf P, Graham TH, Vogt A, Sikorski RP, Ducruet AP, Lazo JS. Cellular analysis of disorazole C1 and structure-activity relationship of analogs of the natural product. Chem Biol Drug Des 2006;67:66–73. [PubMed: 16492150]
21. Yoshida M, Matsui Y, Ikarashi Y, Usui T, Osada H, Wakasugi H. Antiproliferating activity of the mitotic inhibitor pironetin against vindesine- and paclitaxel-resistant human small cell lung cancer H69 cells. Anticancer Res 2007;27:729–736. [PubMed: 17465195]

22. Peterson RH, Meyers MB, Spengler BA, Biedler JL. Alteration of plasma membrane glycopeptides and gangliosides of Chinese hamster cells accompanying development of resistance to daunorubicin and vincristine. Cancer Res 1983;43:222–228. [PubMed: 6847771]
23. Cruz-Monserrate Z, Mullaney JT, Harran PG, Pettit GR, Hamel E. Dolastatin 15 binds in the vinca domain of tubulin as demonstrated by Hummel-Dreyer chromatography. Eur J Biochem 2003;270:3822–3828. [PubMed: 12950266]
24. Hamel E, Covell DG. Antimitotic peptides and depsipeptides. Curr Med Chem Anticancer Agents 2002;2:19–53. [PubMed: 12678750]
25. Erickson LC, Bradley MO, Ducore JM, Ewig RA, Kohn KW. DNA crosslinking and cytotoxicity in normal and transformed human cells treated with antitumor nitrosoureas. Proc Natl Acad Sci U S A 1980;77:467–471. [PubMed: 6928639]
26. Suzuki H, Aoshiba K, Yokohori N, Nagai A. Epidermal growth factor receptor tyrosine kinase inhibition augments a murine model of pulmonary fibrosis. Cancer Res 2003;63:5054–5059. [PubMed: 12941834]
27. Nichols WW, Murphy DG, Cristofalo VJ, Toji LH, Greene AE, Dwight SA. Characterization of a new human diploid cell strain, IMR-90. Science 1977;196:60–63. [PubMed: 841339]
28. Gerhard R, John H, Aktories K, Just I. Thiol-modifying phenylarsine oxide inhibits guanine nucleotide binding of Rho but not of Rac GTPases. Mol Pharmacol 2003;63:1349–1355. [PubMed: 12761345]
29. Folkman J. Angiogenesis: an organizing principle for drug discovery? Nat Rev Drug Discov 2007;6:273–286. [PubMed: 17396134]
30. Kerbel R, Folkman J. Clinical translation of angiogenesis inhibitors. Nat Rev Cancer 2002;2:727–739. [PubMed: 12360276]
31. Isogai S, Horiguchi M, Weinstein BM. The vascular anatomy of the developing zebrafish: an atlas of embryonic and early larval development. Dev Biol 2001;230:278–301. [PubMed: 11161578]
32. Lawson ND, Weinstein BM. Arteries and veins: making a difference with zebrafish. Nat Rev Genet 2002;3:674–682. [PubMed: 12209142]
33. Cross LM, Cook MA, Lin S, Chen JN, Rubinstein AL. Rapid analysis of angiogenesis drugs in a live fluorescent zebrafish assay. Arterioscler Thromb Vasc Biol 2003;23:911–912. [PubMed: 12740225]
34. Vogt A, Cholewinski A, Shen X, Nelson SG, Lazo JS, Tsang M, Hukriede NA. Automated image-based phenotypic analysis in zebrafish embryos. Dev Dyn 2009;238:656–663. [PubMed: 19235725]
35. Lawson ND, Weinstein BM. In vivo imaging of embryonic vascular development using transgenic zebrafish. Dev Biol 2002;248:307–318. [PubMed: 12167406]
36. Molina GA, Watkins SC, Tsang M. Generation of FGF reporter transgenic zebrafish and their utility in chemical screens. BMC Dev Biol 2007;7:62–76. [PubMed: 17553162]
37. Belotti D, Vergani V, Drudis T, Borsotti P, Pitelli MR, Viale G, Giavazzi R, Taraboletti G. The microtubule-affecting drug paclitaxel has antiangiogenic activity. Clin Cancer Res 1996;2:1843–1849. [PubMed: 9816139]
38. Vacca A, Iurlaro M, Ribatti D, Minischetti M, Nico B, Ria R, Pellegrino A, Dammacco F. Antiangiogenesis is produced by nontoxic doses of vinblastine. Blood 1999;94:4143–4155. [PubMed: 10590059]

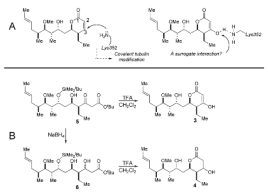

Figure 1. Design and synthesis of pironetin analogs

A. Covalent tubulin modification by αLys352 conjugate addition to bound (−)-pironetin and a pironetin derivative designed to mimic interaction with αLys352 without covalent binding. **B**, Synthesis of pironetin derivatives **3** and **4**.

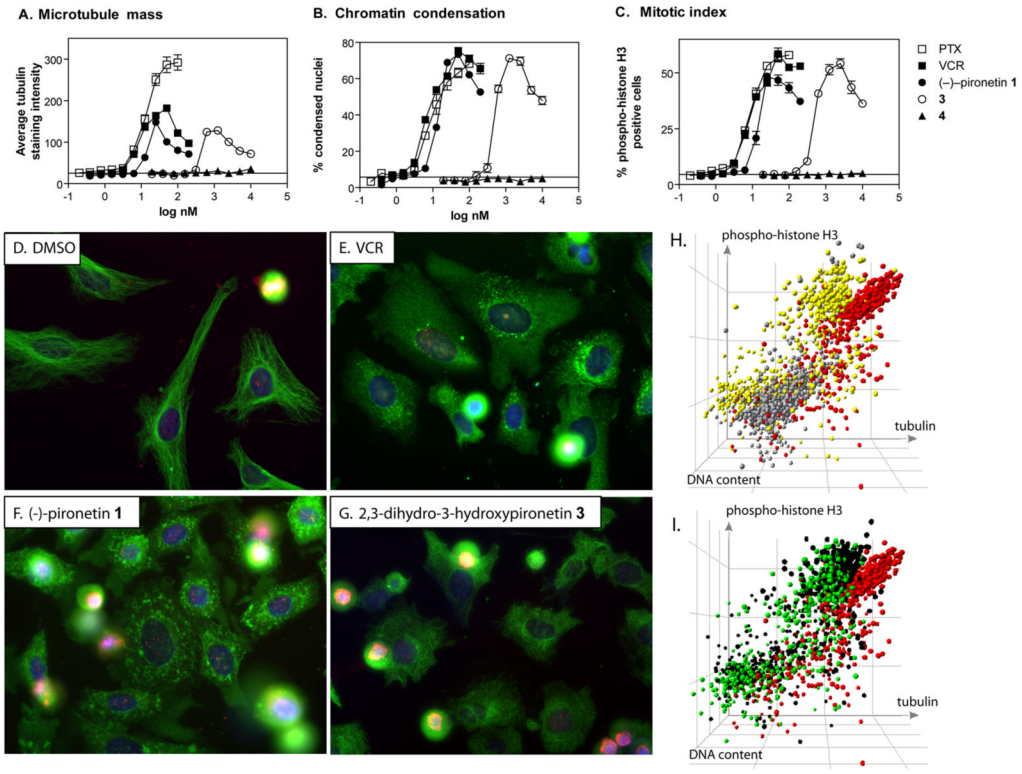

Figure 2. (A–C) High-content analysis of mitotic arrest

HeLa cells were treated with vehicle (dashed line) or ten two-fold dilutions of paclitaxel (□), vincristine (■), (−)-pironetin (●), **3** (○), or **4** (▲) for 21 h and analyzed by high-content analysis for **(A)** microtubule mass, **(B)** condensed nuclei, and **(C)** mitotic index. All agents with the exception of **4** caused arrested cells in mitosis. The microtubule-destabilizing agents vincristine, (−)-pironetin, and **3** showed initial increases in tubulin immunostaining that reversed at higher concentrations. In contrast, tubulin immunostaining increased steadily with the microtubule-stabilizing agent, paclitaxel. Synthetic (−)-pironetin was as potent as vincristine and paclitaxel, whereas **3** was about 20-fold less active. Data are the averages from quadruplicate wells from a single experiment that has been repeated twice with similar results. **(D–G) Microtubule morphology.** Photomicrographs of HeLa cells treated with **(D)** vehicle (DMSO), **(E)** vincristine (200 nM), **(F)** (−)-pironetin (100 nM), or **(G) 3** (1.5 μM), and stained for α-tubulin (green), phospho-histone H3 (red), and nuclei (blue). Vehicle-treated cells have highly organized microtubules and a low percentage of mitotic cells. All agents caused a heterogeneous response of microtubule disorganization and possibly loss of microtubule mass, increased numbers of phospho-histone H3 positive cells, as well as chromatin condensation and nuclear fragmentation. Images shown are representative fields from a single experiment that has been repeated twice with similar results. **(H and I). Loss of tubulin immunostaining in cells treated with microtubule destabilizing agents occurs in both mitotic and non-mitotic cell populations.** Three HCS parameters of cellular activity in 1,000 individual cells were graphically represented using Spotfire Decision Site. **(H)** Vehicle-treated cells (grey) show baseline tubulin staining (x-axis), a low percentage of mitotic cells (y-axis), and 2N DNA content (z-axis). High concentrations of paclitaxel (100 nM, red) caused mitotic arrest and increased microtubule staining due to formation of bright, stable microtubule bundles. In contrast, mitotic and non-mitotic cell populations in vincristine-treated cells (yellow) were shifted to lower tubulin staining intensity compared with paclitaxel, although the loss was more pronounced in the mitotic cells. **(I)** Pironetin (100 nM, green) and **3** (2.5 μM, black) show

mitotic arrest with reduced microtubule staining in the mitotic cells, similar to vincristine (yellow) and different from paclitaxel (red). All axes are logarithmic scale.

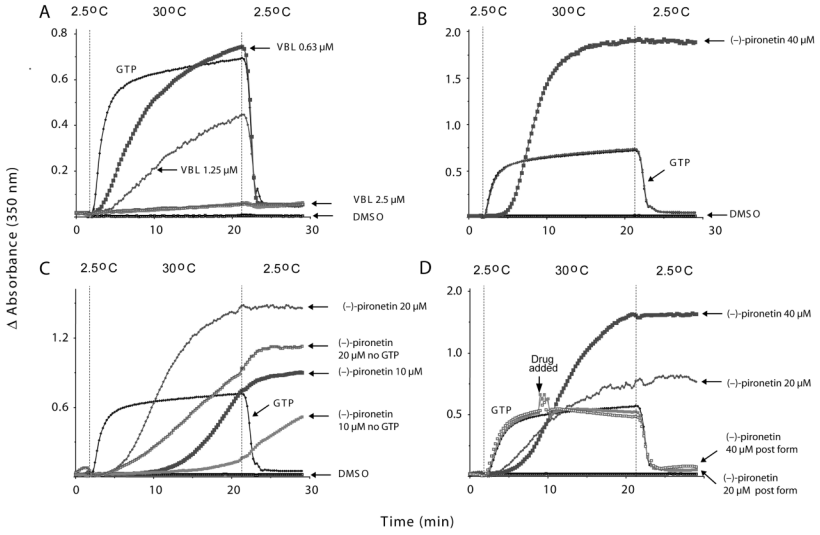

Figure 3. Inhibition of tubulin assembly *in vitro*

Electrophoretically homogenous bovine brain tubulin (final concentration 10 μM; 1 mg/mL) was preincubated with test agents dissolved in DMSO (4% *v*/*v* final concentration) and monosodium glutamate (0.8 M final concentration) for 15 min at 30 °C. The reaction mixture was cooled to 0 °C and GTP (0.4 mM final concentration) was added. Reaction mixtures were transferred to cuvettes held at 2.5 °C in a temperature controlled multichannel spectrophotometer reading absorbance (turbidity) at 350 nm. Baselines were established and temperature was quickly raised to 30 °C (in approximately 1 min). After 20 min, the temperature was returned to 2.5 °C. **(A)** The known microtubule destabilizer, vinblastine (VBL) prevented tubulin assembly in a concentration-dependent manner; **(B)** (−)-Pironetin delayed the onset but increased the extent of tubulin assembly. **(C)** Effect of compound on tubulin assembly in the absence of GTP. Experimental conditions were as above except that to some samples no GTP was added. **(D)** Effect of (−)-pironetin on preformed microtubules. Instead of pre-incubation with test agent, drug in DMSO was added 7 min after initiating GTP-induced assembly.

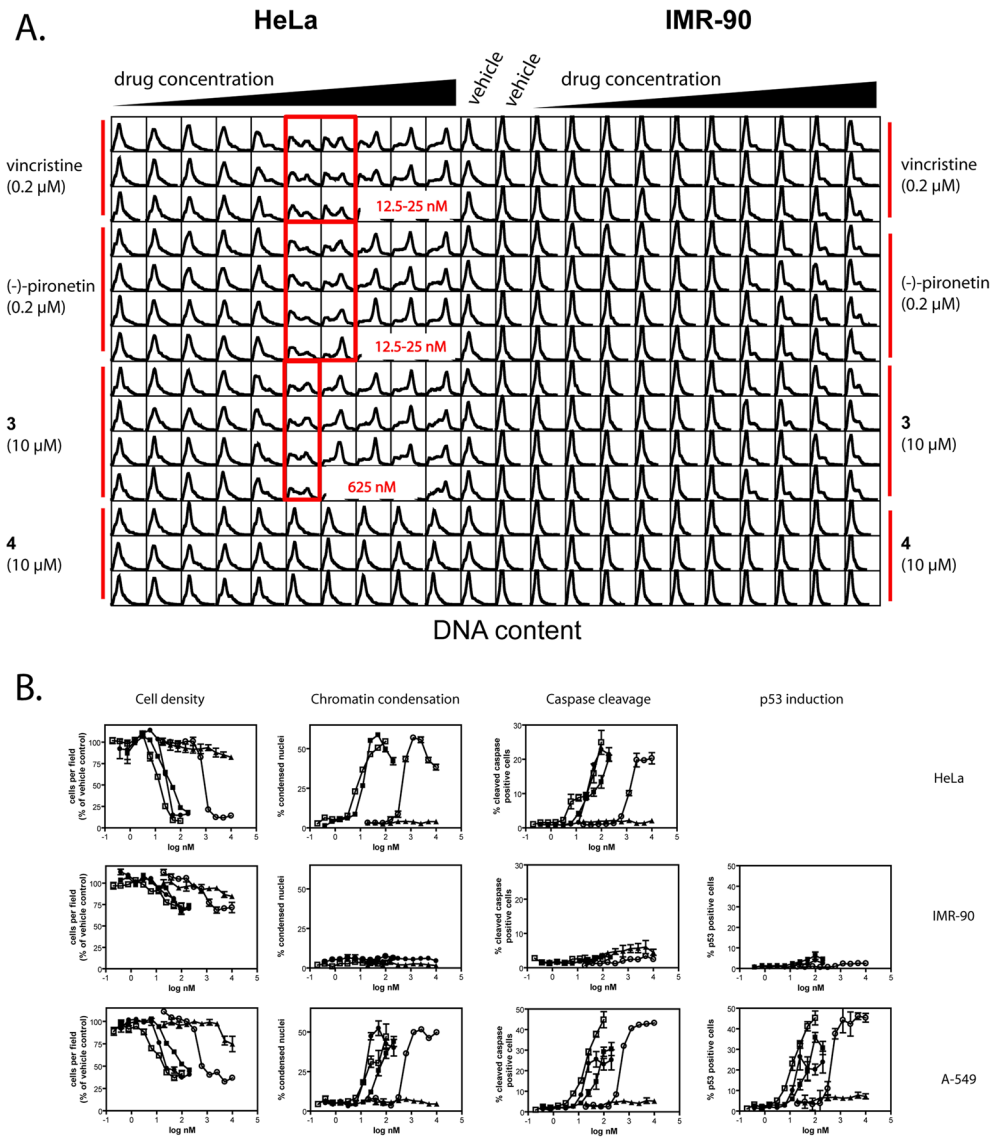

Figure 4. (−)-Pironetin and 3 caused cancer-cell specific apoptosis and cell cycle arrest

HeLa and IMR-90 cells (10,000 per well) were plated on the left and right halves, respectively, of a 384-well microplate. Wells were treated from right to left with 10 two-fold serial dilutions of drugs as shown. The two columns in the center of the plate show 14 replicates of vehicle treated control wells for each cell line. Starting concentrations for each agent are shown in parentheses. **(A) Cell cycle arrest.** Total Hoechst 33342 staining intensities from a minimum of 1,000 cells are presented as DNA content density distributions for each individual well on the microplate. Highlighted are the lowest concentrations where a shift in DNA content could be detected by visual inspection. **(B) High-content analysis of apoptosis.** HeLa, IMR-90, or A-549 cells treated with vehicle or ten two-fold dilutions of paclitaxel (□), vincristine (■), (−)-pironetin (●), **3** (○), or **4** (▲) were analyzed by high-content analysis for cell density, chromatin condensation, caspase cleavage, and p53 induction. Data are the averages of quadruplicate wells from a single experiment that has been repeated at least once with similar results. (HeLa, n=1).

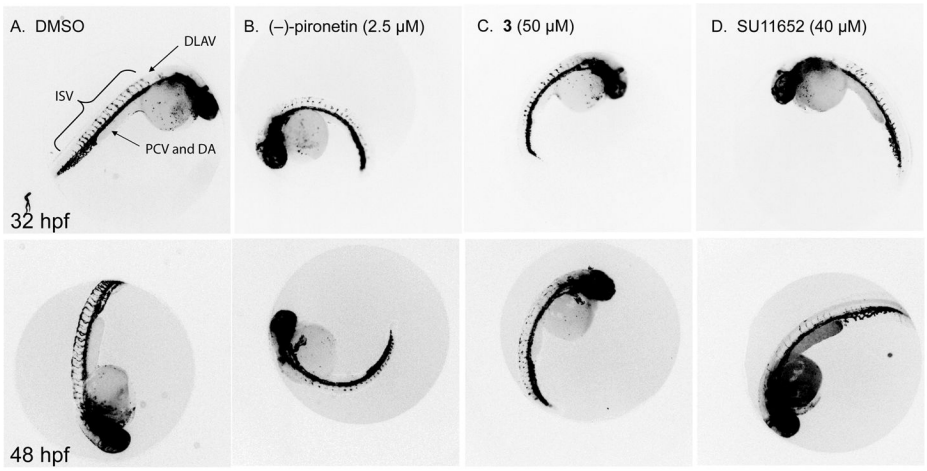

Figure 5. Pironetin and 3 inhibit angiogenesis in zebrafish embryos

Lateral views of 32hpf (*upper panel)* or 48 hpf *(lower panel) Tg(fli1:EGFP)*^{y1} treated with compounds indicated. **(A)** In vehicle treated embryos, intersegmental vessels (ISV) sprout from the dorsal aorta (DA) and connect to the dorsal longitudinal anastomotic vessel (DLAV). **(B)** (−)-pironetin (2.5 μM) prevented the normal outgrowth of ISV and formation of the DLAV. **(C)** At 50μM **3**, ISV growth was stunted in a similar fashion to 2.5 μM (−)-pironetin. These phenotypes are similar to embryos treated with 40μM SU11652, a known VEGFR2 inhibitor **(D)**. Fluorescence images are shown inverted to improve visibility.

Table 1

Antiproliferative activity in human cancer and multidrug-resistant Chinese hamster cells [a]

	MCF-7[b]	T98G[c]	A549[d]	MDA-MB231[d]	DC-3F[d]	VCRd5L[d]	fold resistance [e]
(−)-pironetin	5.0 ± 0.2	7.5 ± 1.2	7.5 ± 0.9	4.6 ± 1.2	9.5 ± 1.2	31 ± 5	3.2
(+)-pironetin	47000 ± 3000	30000 ± 3000	> 5000	> 5000			
4	> 50000	> 50000	> 10000	> 10000			
3	370 ± 40	740 ± 160	179 ± 22	168 ± 65	338 ± 66	1118 ± 56	3.3
vincristine			10.8 ± 2.9	5.5 ± 3.1	19 ± 16	≫ 5000	≫ 250
paclitaxel	10.9 ± 0.2	24.0 ± 9.0	3.5 ± 0.5	1.6 ± 0.9	45 ± 11	2682 ± 109	60

[a] average fifty percent growth inhibitory concentration (GI_{50}) ± SD (nM) from at least three independent experiments

[b] 3-day MTS assay

[c] 4-day MTS assay

[d] 4-day HCS assay

[e] GI_{50} (VCRd5L)/GI_{50} (DC3F)

Table 2

Radioligand binding competition [a]

Compound	% inhibition of [^{3}H]vinblastine binding [b]
vincristine	65 ± 2
dolastatin 10	61 ± 1
colchicine	−11 ± 12
(−)-pironetin (1)	15 ± 4
(+)-pironetin (2)	3 ± 7
3	−6 ± 7
4	−3 ± 8

[a] averages ± SD (nM) from four independent experiments

[b] at 5 μM test agent